^{207,208}Pb$(n, xn\gamma)$ reactions for neutron energies from 3 to 200 MeV

H. Vonach and A. Pavlik
Institut für Radiumforschung und Kernphysik, Universität Wien, A-1090 Wien, Austria

M. B. Chadwick,* R. C. Haight, R. O. Nelson, S. A. Wender, and P. G. Young
Los Alamos National Laboratory, Los Alamos, New Mexico 87545
(Received 9 May 1994)

High-resolution γ-ray spectra from the interaction of neutrons in the energy range from 3 to 200 MeV with ^{207,208}Pb were measured with the white neutron source at the weapons neutron research (WNR) facility at Los Alamos National Laboratory. From these data, excitation functions for prominent γ transitions in ^{200,202,204,206,207,208}Pb were derived from threshold to 200 MeV incident neutron energy. These γ-production cross sections reflect the excitation cross sections for the respective residual nuclei. The results are compared with the predictions of nuclear reaction calculations based on the exciton model for precompound emission, the Hauser-Feshbach theory for compound nucleus decay, and coupled channels calculations to account for direct excitation of collective levels. Good agreement was obtained over the entire energy range covered in the experiment with reasonable model parameters. The results of this work clearly demonstrate that multiple preequilibrium emission has to be taken into account above about 40 MeV, and that the level density model of Ignatyuk, which accounts for the gradual disappearance of shell effects with increasing excitation energy, should be used instead of the Gilbert-Cameron and backshifted Fermi-gas models if excitation energies exceed about 30 MeV. No indication for a reduction of the nuclear moment of inertia below the rigid body value was found.

PACS number(s): 25.40.−h, 24.10.−i, 24.60.Dr

I. INTRODUCTION

Until now, studies of neutron-induced nuclear reactions at energies above about 30 MeV have been restricted mostly to the measurement of total cross sections, elastic scattering, and inclusive particle emission cross sections. Almost no data exist for cross sections of reactions leading to specific exit channels, e.g., cross sections for formation of specific residual nuclei. This is mostly due to the fact that the standard method for this purpose, the activation method, requires monoenergetic neutron sources which do not exist above about 30 MeV.

One way to address this lack of data is to study the prompt γ radiation emitted in neutron-induced reactions using high-resolution Ge detectors. In general, neutron-induced reactions leave the residual nucleus in a highly excited state which subsequently decays via a γ cascade to the ground state in typically three to four steps. The initial intensity distribution over a very large number of highly excited levels is collected in the first few excited levels which then decay to the ground state. Because residual nuclei are mostly formed with relatively high angular momenta, direct transitions to the 0^+ ground states of even-even nuclei are strongly inhibited. In even-even nuclei, often more than 90% of the γ cascades proceed to the ground state (gs) via the first 2^+ levels. Thus the high-resolution measurement of prompt γ production allows the identification of specific residual nuclei by the characteristic γ energies for transitions between low-lying levels, and the determination of effective cross sections for populating these levels. For even-even residual nuclei, we get approximately the total production cross section by measuring the first 2^+-to-ground-state γ-ray transition. The partial cross sections not included in this measurement result from those γ rays in the cascade that bypass the first 2^+ excited state, and those reactions that leave the residual nucleus directly in the ground state.

This technique can also be used when the residual nucleus is not even-even. In this case the partial production cross sections are obtained from the production cross sections for a given γ-ray transition, and the total production cross section must be deduced through nuclear model calculations. The partial cross section itself is of interest because it indicates the population of an individual state in the same sense as the production of isomeric states. Here, however, the states have short half-lives, whereas the less numerous isomeric states have long half-lives.

With a pulsed white neutron beam covering a large energy range, this method has the additional advantage that many cross sections can be measured simultaneously over a large incident neutron energy range in one experiment. The neutron energy is determined by time of flight, and the prompt γ radiation is measured by means of a high-resolution Ge detector.

With the availability of the weapons neutron research (WNR) facility [1] it is possible to extend such measure-

*Present address: Lawrence Livermore National Laboratory, Livermore, CA 94551.

 ©1994 The American Physical Society

ments to much higher energies (several hundred MeV) than made previously at electron linear accelerators [2,3]. Preliminary tests demonstrated that identification and measurement of individual γ lines are possible at incident energies of several hundred MeV in spite of the complexity of the spectra. In order to test present nuclear reaction models (which were developed at lower energies) over a wider energy range, we measured the prompt γ radiation for a few specific nuclei from threshold to the highest incident neutron energy feasible.

^{207,208}Pb samples were selected for a comparison between theory and experiment because a large amount of data already exists to restrict the parameter space for the nuclear model calculations. This data base can be hoped to reduce considerably the ambiguities inherent in comparisons of experimental results with calculations depending on many parameters. In addition, in the ^{208}Pb region there are very large shell effects in the nuclear level density, and it is thus possible to study the dependence of these shell effects on excitation energy with high sensitivity. Finally, there exists very good spectroscopic information on the discrete levels and γ-branching ratios for all lead isotopes reached by (n,xn) reactions up to $x = 9$ (^{200}Pb). This information is important for a correct interpretation of the measured γ-production cross sections.

The present article describes measurements of the prompt γ radiation from the interaction of neutrons from the WNR beam with isotopically enriched samples of ^{207,208}Pb as a function of neutron energy. These data were acquired in a two-parameter, E_n (from neutron time of flight) and E_γ (from γ-ray pulse height), experiment. The first part of the analysis of these γ spectra deals with the excitation functions of the most prominent γ transitions, that is, the $2_1^+ \rightarrow$gs transitions observed in ^{200,202,204,206}Pb, the $(\frac{3}{2})_1^- \rightarrow$gs and $(\frac{5}{2})_1^- \rightarrow$gs transitions in ^{207}Pb, and the $3_1^- \rightarrow$gs transition in ^{208}Pb. Section II describes the experiment, Sec. III reports the procedures used in deriving γ-production cross sections from the raw data, Sec. IV describes the nuclear reaction calculations and the choices for the model parameters, and in Sec. V the experimental and theoretical results are presented, compared, and discussed.

II. EXPERIMENT

The experiments were performed on the 30° left flight path of the WNR facility, which is described in detail in Ref. [1]. The general features of the 30° left Ge spectrometer setup and of the beam pulse structure are described in Ref. [4]. A schematic diagram of the flight path collimation and shielding is shown in Fig. 1. The Pb samples were mounted at a distance of 41.48 m from the neutron production target on a thin plastic frame that was suspended from a steel rod. The samples were oriented at 45° with respect to the neutron beam to reduce the attenuation of the γ rays in the sample for detectors positioned at 90° and 125°. The shape of the beam spot at the sample position was an 8.4 cm diameter circle. A scan of the beam using a 6 mm diameter plastic scintillator showed the beam profile to have good uniformity and good edge definition. The beam dump is well shielded and located 10 m behind the sample position.

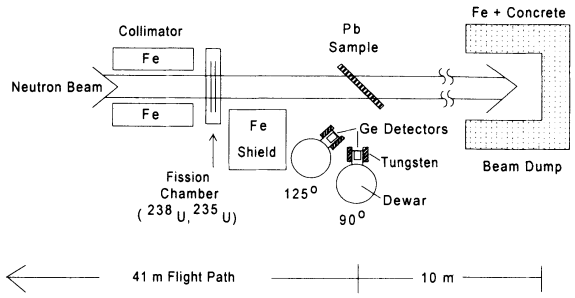

FIG. 1. Experimental setup.

The ^{208}Pb sample consisted of a flat plate, 1.6 mm thick, in an oval shape, approximately 9.1 cm wide and 6.6 cm high, weighing 116.3 g. The oval sample, rotated at 45° with respect to the neutron beam, covered a projected area smaller than the beam spot size. In order to measure the contribution to the cross sections from secondary particle production and multiple reactions, the sample was subsequently rolled out to a thickness of 0.6 mm and cut into two pieces. Data were taken with a single thin plate, and also with both thin plates mounted together. In the measurements with the thinner plates, some portions of the samples were outside of the beam envelope. Due to the odd shape of the rolled samples it was difficult to determine precisely how much of the sample was in the beam.

The 85.64 g ^{207}Pb sample was in the form of three irregular oval plates, each with a thickness of 0.23 mm. The three plates were mounted together for a total thickness of 0.69 mm. The isotopic composition of the samples as reported by the supplier, Oak Ridge National Laboratory, is given in Table I.

To determine the absolute normalization of the cross sections, an experiment was performed at the Institute of Physics of the Slovak Academy of Sciences in Bratislava, Slovakia [5,6] in which data were acquired at $E_n = 14.7$ MeV. The normalization of the data is discussed in Sec. III.

Two high-purity coaxial Ge detectors were used in each experiment. The detectors had active volumes of approximately 70 cm^3 and 140 cm^3 for the 90° and 125° detectors, respectively. The collimation for each detector consisted of approximately 40 kg of tungsten powder contained in a thin-walled cylindrical steel tube with plastic end caps and an inner plastic tube. The volume contain-

TABLE I. Isotopic composition of the Pb samples.

Isotope	^{207}Pb sample	^{208}Pb sample
^{204}Pb	<0.05%	<0.01%
^{206}Pb	2.53%	0.28%
^{207}Pb	92.78%	<0.15%
^{208}Pb	4.69%	>99.56%

ing the tungsten powder had an inner diameter of 9.5 cm, an outer diameter of 15 cm, and was 28.5 cm long. The density of the powder was approximately 13 g/cm^3. These shielding materials were chosen instead of lead because Pb shielding is excited by scattered neutrons and emits the same γ rays as the isotopic lead targets. There was no iron inside the collimators because the setup was also used for measurements on isotopic Fe samples.

The detectors were positioned 40.0 cm from the sample center at 90° and 27.1 cm from the sample at 125°. The detector and collimator assemblies were positioned side by side to take advantage of the better shadow shielding on one side of the beam. The sample-to-detector distance was chosen to maximize the count rate while keeping the effects of pileup at a reasonable level for the 125° detector. The sample-to-detector distance for the 90° detector was constrained by the physical contact of the two collimators. One of the detectors was positioned at 125° because the value of the P_2 Legendre polynomial function is zero at that angle. The usual expansion of the γ-ray angular distribution in terms of Legendre polynomials is

$$A_0[1 + a_2P_2(\cos\theta) + a_4P_4(\cos\theta) + \cdots] .$$

For $E2$ (e.g., $2_1^+ \rightarrow$gs) transitions, the angle-integrated cross section can be approximated as 4π times the measured cross section at $\theta = 125°$, provided a_4 is small. Data from the 90° detector were not used in the analysis or results given here. The detector efficiencies (including the solid angle) were measured by placing calibrated ^{56}Co, ^{60}Co, ^{88}Y, ^{137}Cs, and ^{152}Eu sources at the sample center position.

Data were taken with the Pb samples removed for background determination. Such measurements, however, do not account for background γ rays produced by neutrons which are scattered from the sample into the collimators and detectors. To get an estimate of this background, a measurement was performed with a 0.5 mm thick tantalum plate at the sample position. The background spectra did not show any γ-ray lines overlapping in energy with the γ rays analyzed from the ^{207,208}Pb$(n, xn\gamma)$ reactions.

The neutron flux was measured with a fission chamber. The design of the fission chamber is described in Ref. [7]. The chamber contained both ^{235}U and ^{238}U fission foils. The fission chamber was centered on the beam at a distance of 37.30 m from the production target, and the active fission deposit covered the entire neutron beam.

The electronics used were fairly standard. The slow risetime rejection feature of the Ortec 473A constant fraction discriminators was used to improve the time resolution of the system. Despite efforts to minimize such effects, the time resolution was somewhat dependent on the pulse height. The time resolution, determined from the γ-ray flash, varied from 10 ns full width at half maximum (FWHM) for $E_\gamma = 200$ keV to approximately 5 ns FWHM for $E_\gamma = 3$ MeV. The intrinsic time width of the γ-ray flash from the neutron source is typically less than 300 ps FWHM. The γ-ray energy resolution obtained during the experiments was 2.8 keV FWHM for the 125° detector at a γ-ray energy of 803 keV. The γ-ray energy resolution was limited in part by the selection of a 1 μs pluse-shaping time constant which allowed a fast counting rate without excessive pileup.

Data were acquired using the XSYS data acquisition and analysis computer program [8]. The neutron time of flight (TOF) was measured using a Lecroy (LRS) 4204 time-to-digital converter (TDC), and the γ-ray pulse height (PH) was digitized using an LRS 3512 analog-to-digital converter. The LRS 4204 TDC has excellent differential and integral linearity and time base stability. Both converters were coupled to buffer memories to store the data in the CAMAC crate during beam bursts. Data were read out between beam bursts, stored in event mode on disk, and sorted into one-dimensional (1D) and 2D spectra. The 2D spectra consisted of 512 (TOF) channels by 4096 (PH) channels.

III. DATA REDUCTION

Four measurements were performed, one with a ^{207}Pb sample and three with ^{208}Pb samples. Samples of various thicknesses, as described above, were used in the ^{208}Pb runs to estimate correction factors for finite sample size effects.

The γ-ray transitions analyzed in this work are listed in Table II. From the measurements with the ^{207}Pb sample, only the 803.1-keV, 960.7-keV, and 1026.5-keV transitions in ^{206}Pb, ^{202}Pb, and ^{200}Pb, respectively, were analyzed. The 569.7-keV and 897.8-keV transitions from the ^{207}Pb$(n, n'\gamma)$ reaction were not analyzed because low-energy neutrons from the preceding micropulse (frame overlap) gave significant contributions to the measured γ-production cross sections. Due to the high excitation energy (2614.6 keV) of the first excited level of ^{208}Pb, the frame-overlap problem did not occur in studying the ^{208}Pb$(n, n'\gamma)$ reaction.

The first step in the data analysis was to divide the neutron energy range from 3 to 200 MeV into 53 groups with increasing group widths (0.25–20 MeV) according to the energy resolution of the experiment. The neutron fluence for each energy group was determined from the two-dimensional (neutron TOF versus fission PH) fission chamber spectra [7]. Photofission events induced by γ rays emitted from the neutron production target were used as a time reference to signal the arrival of the proton beam pulse at the neutron production target. The time scale was calibrated by a time calibrator with a quartz oscillator. Alpha particles and fission fragments were distinguished by their pluse heights. A time-uncorrelated random background present in the TOF spectra was subtracted prior to sorting the fission events into neutron energy groups. The neutron fluence for each group was calculated using the cross sections for the ^{235}U(n, f) and ^{238}U(n, f) reactions given by Lisowski *et al.* [9].

Two-dimensional spectra, neutron TOF versus γ pulse height, were recorded for the Ge detector. The "γ flash" from the neutron production target was used as a time reference. For each neutron energy group a one-dimensional γ pulse-height spectrum was derived from the two-dimensional spectrum. Figure 2 shows two γ

TABLE II. Nuclear reactions and γ transitions investigated in this work.

Reaction	γ transition investigated	Energy (keV)	Isomers in residual nucleus $J\pi$	E (keV)	$t_{1/2}$	γ energy characteristic for isomer decay (keV)	Measured γ-production cross section
^{207}Pb($n,2n\gamma$)^{206}Pb	$2^+ \rightarrow 0^+$(gs)	803.1	12^+	4027.0	197 ns		
			7^-	2200.2	125 μs	516.2	$\sigma(803.1) - \sigma(516.2)$
^{207}Pb($n,6n\gamma$)^{202}Pb	$2^+ \rightarrow 0^+$ (gs)	960.7	12^+	3103.4	200 ns		
			7^-	2208.5	42 ns	657.5[b]	
			9^-	2169.8	3.53 h	787.0	$\sigma(960.7) - \sigma(657.5) - \sigma(787.0)$
^{207}Pb($n,8n\gamma$)^{200}Pb	$2^+ \rightarrow 0^+$ (gs)	1026.5	12^+	2980	194 ns		
			9^-	2176	480 ns		
			7^-	2153.7	44 ns	245.1	$\sigma(1026.5) - \sigma(245.1)$
^{208}Pb($n,n'\gamma$)^{208}Pb	$3^- \rightarrow 0^+$ (gs)	2614.6		none			$\sigma(2614.6)$
^{208}Pb($n,2n\gamma$)^{207}Pb	$\frac{5}{2}^- \rightarrow \frac{1}{2}^-$ (gs)	569.7	$\frac{13}{2}^+$	1633.4	0.805 s	1063.7	$\sigma(569.7) - \sigma(1063.7)$
^{208}Pb($n,3n\gamma$)^{206}Pb	$2^+ \rightarrow 0^+$ (gs)	803.1	12^+	4027.0	197 ns		
			7^-	2200.2	125 μs	516.2	$\sigma(803.1) - \sigma(516.2)$
^{208}Pb($n,5n\gamma$)^{204}Pb	$2^+ \rightarrow 0^+$ (gs)	899.1[a]	7^-	2264.2	450 ns		
			9^-	2185.7	67.2 min		
			4^+	1273.9	265 ns	374.7	$\sigma(899.1) + \sigma(897.8) - \sigma(374.4)$[a]
^{208}Pb($n,7n\gamma$)^{202}Pb	$2^+ \rightarrow 0^+$ (gs)	960.7	12^+	3103.4	200 ns		
			7^-	2208.5	42 ns	657.5[b]	
			9^-	2169.8	3.53 h	787.0	$\sigma(960.7) - \sigma(657.5) - \sigma(787.0)$
^{208}Pb($n,9n\gamma$)^{200}Pb	$2^+ \rightarrow 0^+$ (gs)	1026.5	12^+	2980	194 ns		
			9^-	2176	480 ns		
			7^-	2153.7	44 ns	245.1	$\sigma(1026.5) - \sigma(245.1)$

[a]The 899.1-keV ($2^+ \rightarrow 0^+$ in ^{204}Pb) and 897.8-keV [$(3/2)^- \rightarrow (1/2)^-$ in ^{207}Pb] γ lines were not resolved.
[b]This line was not resolved from the 657.2-keV ($5^- \rightarrow 4^+$) transition in ^{206}Pb. A correction was made using the results of model calculations.

spectra from the ^{208}Pb sample for the neutron energy ranges 13–15 MeV and 100–200 MeV.

The number of counts in the γ-peak areas was obtained by adding the channel contents within the peak and subtracting a smooth background. The background under a peak was obtained from polynomials fitted to suitable background regions on both sides of the peak. A linear background was used for all γ lines with the exception of the 569.7-keV transition in ^{207}Pb, where the background could be fitted better by a quadratic polynomial.

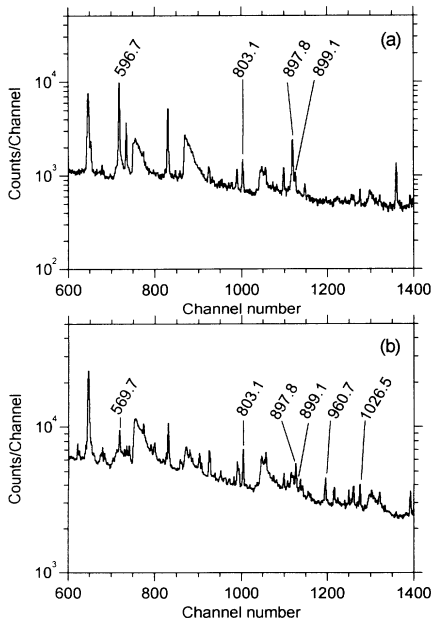

FIG. 2. γ spectrum from the interaction of fast neutrons with ^{208}Pb: (a) E_n =13–15 MeV; (b) E_n =100–200 MeV.

As the choice of the peak limits and the background region is somewhat subjective, an additional uncertainty component was added quadratically to the statistical uncertainties. An estimate of this uncertainty was obtained by comparing the peak areas determined by different summing limits.

From the peak areas, the neutron fluence, and the γ-detector efficiency, relative excitation functions were derived for each γ transition analyzed. The differential cross sections at $\theta = 125°$ were converted to total γ-production cross sections by multiplying them by 4π as discussed in Sec. II. Corrections were applied for the attenuation of the γ rays within the samples and for contributions of secondary neutrons to the γ-production cross sections. The correction factors for γ-ray absorption were calculated using absorption cross sections from Ref. [10].

Because of uncertainty in our knowledge of the Ge detector dead time and the absolute flux intercepted by the irregularly shaped samples, the relative cross sections were normalized to data obtained in a separate measurement [5]. To perform the normalization, the cross sections measured at WNR with a neutron energy of 14.5 MeV (energy group 14–15 MeV) were converted to E_n = 14.7 MeV for comparison with the results of the 14.7-MeV experiment using the slope of the excitation functions. For the ^{207}Pb($n,xn\gamma$) reac-

tions the normalization factor was derived from the cross section of the 803.1-keV transition in ^{206}Pb. For each run of the ^{208}Pb$(n, xn\gamma)$ measurements, the normalization factor was calculated from the γ production cross sections of the 569.7-keV (569.7 keV$\rightarrow$gs), 897.8 keV (897.8 keV$\rightarrow$gs), 1094.6-keV (2728$\rightarrow$1633.4 keV), and 1770.2-keV (2339.9$\rightarrow$569.7 keV) transitions in ^{207}Pb, and from the 583.2-keV (3197.7$\rightarrow$2614.6 keV) and 2614.6-keV (2614.6 keV$\rightarrow$gs) transitions in ^{208}Pb. The results of each of the three measurements with ^{208}Pb samples were normalized and the final cross sections for the ^{208}Pb$(n, xn\gamma)$ reactions were obtained by weighted averaging of the normalized results of the three individual measurements.

Multiply scattered neutrons can give significant additional contributions to the measured cross sections at high incident neutron energies, especially for reactions with low thresholds. To estimate the correction factors for this effect, we assumed that the correction factor $f(E_n)$ can be expressed as $f(E_n) = 1 + c(E_n)x$, with $c(E_n)$ an energy-dependent factor, and x the sample thickness. Under the assumption that there is no correction necessary for neutron energies just above the reaction threshold, $c(E_n)$ was determined form the ratios of the peak areas measured with ^{208}Pb samples of different thicknesses. The factor $c(E_n)$ was calculated for each energy group, and the $c(E_n)$ values used for the calculation of the correction factors were obtained from a smooth polynomial fit to these data. Two cases where the correction factors are large, are the 2614.6-keV line [^{208}Pb$(n, n'\gamma)$ reaction] and the 569.7-keV line [^{208}Pb$(n, 2n\gamma)$ reaction]. In these cases, the correction factors were calculated to be as large as 60% and 25%, respectively, for neutron energies above 150 MeV and a 1.2 mm thick sample. The $c(E_n)$ values determined for the ^{208}Pb$(n, 2n\gamma)$ reaction were also used to calculate correction factors for the γ radiation produced by the ^{207}Pb$(n, 2n\gamma)$ reaction. No corrections for the effect of secondary neutrons were applied to the γ lines from reactions with higher thresholds, as no effect was found by analyzing the 803.1-keV line from the ^{208}Pb$(n, 3n\gamma)$ reaction using the different sample thicknesses.

The analysis is more complicated when isomeric states ($t_{1/2} > 2$ ns) are involved in the cascade. When isomers are present in the cascade, the γ radiation from the first excited level $\rightarrow$gs is not emitted promptly. Such delayed transitions may be detected in this type of experiment, but they cannot be properly correlated with the neutron energy because the measured TOF includes the decay delay. Therefore correction procedures had to be applied to ensure that the derived cross sections relate only to the prompt emission of γ rays. The cross sections associated with the prompt part of the γ cascade are the production cross sections for the relevant transitions minus the contributions from the long-lived isomers. According to the level schemes and γ-ray intensities [11] of ^{200,206,207}Pb, where there is more than one isomeric state, all of the known higher-lying isomeric states decay to the lowest-energy isomer. Thus the γ-decay cross section for the lowest-energy isomer equals the sum of the population cross sections of all isomers. For ^{204}Pb this is also valid to better than 2%. The relevant decay schemes are shown in Fig. 3.

For the residual nuclei, the prompt γ-production cross sections for the first excited state$\rightarrow$gs transitions can be expressed as differences of the production cross sections for individual transitions as listed in the last column of Table II. A special case is the $2_1^+ \rightarrow 0_1^+$ transition in

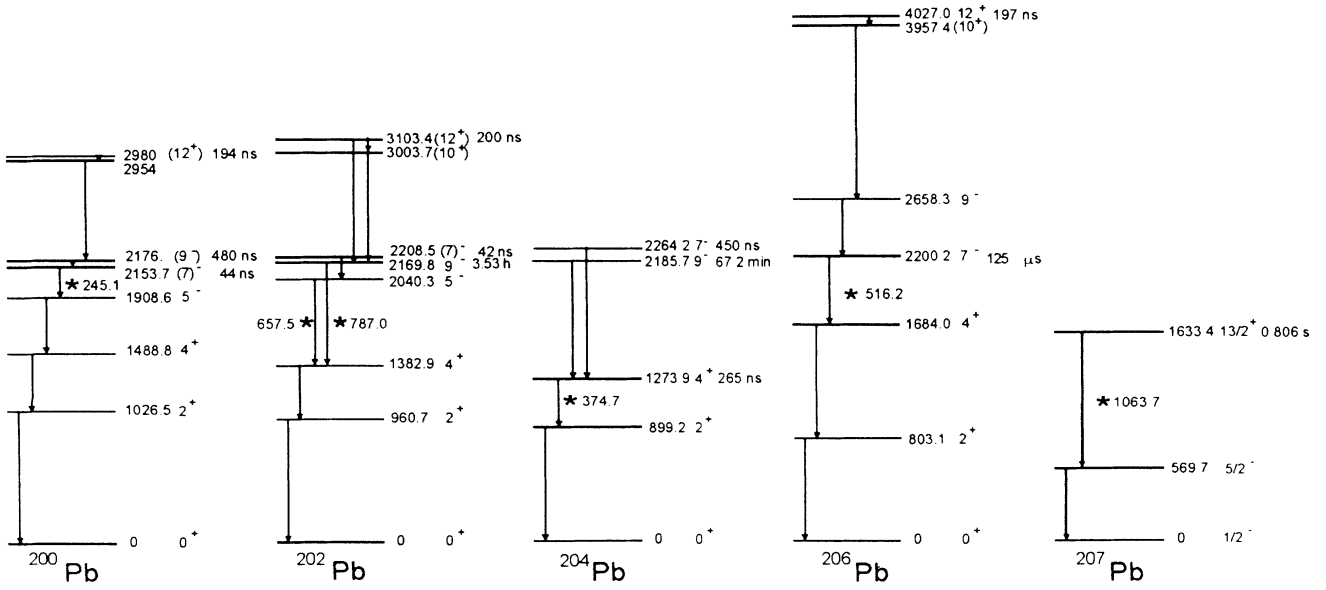

FIG. 3. Level diagrams of the Pb isotopes investigated showing major transitions from long-lived ($t_{1/2} > 2$ ns) isomers. Asterisks indicate the transitions used in the analysis to subtract the long-lived component of the decay (see Sec. III). Numbers to the right of the levels are the excitation energies in keV, spins and parities, and $t_{1/2}$ of the long-lived isomers. Numbers by the asterisks are the gamma-ray energies of the transitions. Data are from Ref. [11].

^{204}Pb (E_γ = 899.1 keV), which was not resolved from the E_γ = 897.8-keV $(\frac{3}{2})_1^-$ →gs transition in ^{207}Pb. The $(\frac{3}{2})_1^-$ state in ^{207}Pb is not fed by the single isomeric state in ^{207}Pb, and therefore we report the sum of these two cross sections minus the contribution from the 1273.9 keV 4^+ isomer of ^{204}Pb.

A more complicated situation exists in the residual nucleus ^{202}Pb. According to Ref. [11] there are three isomers with excitation energies 3103.4, 2208.5, and 2169.8 keV. (See Fig. 3.) The 3103.4-keV level decays completely to the 2169.8-keV isomer. The latter decays with a probability of 99.6% to the first excited 2^+ level via a γ cascade starting with a 787.0-keV transition. The 2208.5-keV isomer decays with 95.6% probability to the 2040.3-keV level. This 168.1-keV transition was below our threshold. Therefore we analyzed the 657.5-keV transition from the 2040.3-keV level to the 1382.9-keV level instead. Its production cross section was subtracted from the observed $2_1^+ \rightarrow 0_1^+$ cross section. As the 2040.3-keV level is not exclusively fed by the decay of the 2208.5-keV isomer, the measured quantity for the $2_1^+ \rightarrow 0^+$ (gs) transition is not the prompt part of this transition but only a fraction of it.

All of these measured partial cross sections (last column of Table II) are suitable quantities for direct comparison with the results of model calculations (see Sec. V). The influence of some weaker transitions in the decay of the isomers of ^{202}Pb and ^{204}Pb was neglected because their effect is small compared to the uncertainties of this experiment and the general accuracy of nuclear model calculations.

The actual correction of the measured γ-production cross sections for the delayed contributions depended on the half-lives of the various isomers. If the lifetime of the isomer is large compared to the duration of a macropulse (typically 800 μs), most of the delayed γ rays (about 98%) will be emitted between the macropulses when the detector electronics is gated off, and thus will not be counted. Therefore the contribution from the decay of the 1633.4-keV $(\frac{13}{2})^+$ isomer in ^{207}Pb ($t_{1/2}$ = 0.805 s) to the measured γ-production cross section of the 569.7-keV line, and the contribution of the 2169.8-keV 9^- isomer in ^{202}Pb ($t_{1/2}$ = 3.53 h) was neglected.

For isomers with half-lives comparable to the duration of a macropulse, the delayed γ rays are observed in the measured spectra with a uniform distribution in time, and can be subtracted as a constant background. The background rate was determined from the data below the reaction threshold. This method was used to correct for the contribution of the 2200.2-keV 7^- isomer ($t_{1/2}$ = 125 μs) in ^{206}Pb.

For the remaining isomers with half-lives in the range from 40 to 300 ns, the delayed contributions to the measured $2_1^+ \rightarrow 0^+$ (gs) transitions were determined from the time distributions of the decay of the corresponding isomer. To correct for the delayed parts of the $2_1^+ \rightarrow 0^+$ transitions in ^{200}Pb, ^{202}Pb, and ^{204}Pb, the 245.1-keV, 657.5-keV (as stated above, this transition is partly prompt), and 374.7-keV lines, respectively, were analyzed. These γ transitions are observed with the same delay time distributions and the same production cross sections as the parts of the $2_1^+ \rightarrow 0^+$ transitions in ^{200}Pb and ^{204}Pb that are fed via the 7^- and the 4^+ isomer, respectively. In each time bin the intensities of these lines were subtracted from the corresponding $2_1^+ \rightarrow 0^+$ intensities.

Following these corrections, the cross sections at neutron energies below the reaction thresholds were zero within the experimental uncertainties. This indicates that the correction procedures and assumptions are correct.

Due to the 92.78% enrichment of the ^{207}Pb sample, the measured cross sections had to be corrected for contributions from ^{208}Pb and ^{206}Pb present in the sample. These corrections were made using the measured ^{208}Pb($n, xn\gamma$) cross sections and the results of model calculations performed with the code GNASH [12] for ^{206}Pb.

To estimate the final uncertainties of the γ-production cross sections, all statistical and systematic uncertainty components were combined according to the rules of error propagation. The contribution from the normalization procedures to the total uncertainty was about 12% for the ^{207}Pb($n, xn\gamma$) cross sections and about 10% for the ^{208}Pb($n, xn\gamma$) cross sections.

IV. CROSS SECTION CALCULATIONS

Extensive calculations of the γ-ray production cross sections studied experimentally were performed by means of the computer code GNASH [12], which describes the precompound mechanism of nuclear reactions by the exciton model, and compound nucleus decay by the Hauser-Feshbach model, and allows the addition of contributions from direct reactions. The aim of the cross section calculations was not to reproduce the experimental results merely by varying a large number of parameters but to test the ability of the simple exciton precompound model [14] (including surface effects [15]) and the Hauser-Feshbach model of compound nuclear reactions to describe cross sections for specific reaction channels at higher energies than have been considered in the past. Calculations of ($n, xn\gamma$) cross sections for particular γ-ray transitions provide exacting tests of the nuclear models because such transitions select only a part of the angular momentum distribution involved in the overall reaction process.

Most model parameters were not varied but were kept at values typical of a large number of analyses of a variety of data at lower energies. For example, the matrix element normalization constant that describes the competition between precompound particle emission and internal transitions to higher exciton states in preequilibrium emission was fixed at a typical value of 135 MeV^3. Likewise, the nuclear single-particle state densities were set to $A/13$ MeV^{-1} in the asymptotic limit where shell effects are washed out, and a standard formulation by Kopecky and Uhl [16] was utilized for the γ-ray strength functions.

The choice of the optical model potential was restricted by the condition that it has to reproduce both total neutron and total reaction cross sections over the whole energy range covered by our experiment. Accordingly,

TABLE III. Deformed optical model potential for ^{208}Pb+n calculations over the neutron energy range 1 keV$\leq E_n \leq$ 200 MeV. V_R: strength of the real potential; W_d: strength of the derivative part of the imaginary potential; W_V: strength of the volume part of the imaginary potential; V_{SO}: strength of the spin-orbit potential; r_R and a_R: radius and diffuseness of the respective Woods-Saxon distributions.

Well depth (MeV)		Geometry (fm)	
$V_R = 50.04 - 0.279E_n$	$(0 < E_n < 60$ MeV)	$r_R = 1.183$	$a_R = 0.6966$
$= 111.0925 - 19\ln E_n$	$(60 \leq E_n \leq 200$ MeV)		
$W_d = 1.00 + 0.2502E_n$	$(0 < E_n < 14$ MeV)	$r_R = 1.273$	$a_R = 0.699$
$= 5.722 - 0.08705E_n$	$(14 \leq E_n \leq 65.7$ MeV)		
$= 0$	$(65.7 \leq E_n \leq 200$ MeV)		
$W_V = 0$	$(0 < E_n < 14.4$ MeV)	$r_R = 1.273$	$a_R = 0.699$
$= -2.60 + 0.18E_n$	$(14.4 \leq E_n \leq 40$ MeV)		
$= 2.20 + 0.06E_n$	$(40 \leq E_n \leq 100$ MeV)		
$= 8.20$	$(100 \leq E_n \leq 200$ MeV)		
$V_{SO} = 6.18$	$(0 < E_n < 200$ MeV)	$r_R = 1.16$	$a_R = 0.677$

the coupled-channels neutron potential by Shamu and Young [17], obtained for experimental neutron data in the energy range from 8.5 to 10 MeV, was modified and extended to both lower and higher neutron energies by matching the available experimental neutron total, elastic scattering, and nonelastic scattering cross section data. For the extension of the coupled-channels analysis to higher energies, the one-channel (or spherical) optical model potential of Schutt *et al.* [18] was used as a guide. The coupled-channels code ECIS [19] was used with relativistic kinematics for all calculations. The potential that resulted, which is presented in Table III, gives a reasonable representation of the available neutron total, elastic, and nonelastic scattering cross section data to approximately 200 MeV (note that a more detailed extension of the coupled-channels analysis by Shamu and Young is in progress [20]). For the proton channel, the global potential of Becchetti and Greenlees [21] was utilized to proton energies of 50 MeV, and the potential of Madland [22] was used at higher energies.

Information on discrete levels (energies, spins, parities, and branching ratios) was taken from the Evaluated Nuclear Structure Data File (ENSDF) [11]. The number of discrete levels and the corresponding excitation energy ranges for the various residual nuclei in the calculations are given in Table IV. Direct collective excitation also was considered for a number of levels in ^{208}Pb, and was accounted for by the coupled-channels calculations described above. As described in detail in Ref. [17], all ^{208}Pb states below an excitation energy of 10 MeV that are known from alpha, proton, and/or electron inelastic scattering experiments to be highly collective were included in the calculations. Specifically, one-phonon excitations were assumed for the discrete states at 2615 (3^-), 4085 (2^+), 4323 (4^+), 4424 (6^+), and 4610 (8^+) keV, and a cluster of low-energy octupole resonance (LEOR) states represented by a single 3^- state at 5380 keV. Deformation parameters were taken from distorted-wave Born approximation (DWBA) analyses of proton-induced measurements for the states below 5 MeV excitation energy [11], and the deformation for the LEOR state at 5380 keV was scaled from the 3^- state at 2615 keV [17].

For the nuclear level densities, the Ignatyuk model [23] was chosen instead of the simpler Gilbert-Cameron [24] and other Fermi-gas models that incorporate an energy-independent level density parameter. By the use of this energy-dependent level density parameter, the Ignatyuk model includes the theoretically expected disappearance of shell effects in the nuclear level densities at higher excitation energies, such as those covered in the present experiment. Within this model the nuclear moment of inertia was given the value of the full rigid body moment of inertia. The level density parameters were chosen using the systematics of Young *et al.* [25], and adjustments were made to the pairing energies based on measurements of $(n, 2n)$ cross sections near threshold for the various isotopes of Pb.

Three extensions on the modeling of preequilibrium reactions were installed in GNASH to improve the physics for calculations at higher energies. Until now the emission of only one preequilibrium particle has been included in the code. That is, previously it was assumed that, after the first preequilibrium particle is emitted, the remaining particle-hole states proceed to equilibrium via a series of nucleon-nucleon collisions before decaying. We have modified this assumption to allow the particle-hole states left after primary preequilibrium emission to de-

TABLE IV. Maximum excitation energies and numbers of discrete states included for the various residual nuclei in the ^{208}Pb+n calculations.

Residual nucleus	Maximum excitation energy (MeV)	Number of states
^{209}Pb	3.078	22
^{208}Pb	5.147	60
^{207}Pb	4.996	78
^{206}Pb	3.602	34
^{205}Pb	2.3104	36
^{204}Pb	3.2406	49
^{203}Pb	2.8336	43
^{202}Pb	3.0217	29
^{201}Pb	2.7966	40
^{200}Pb	2.7732	13
^{199}Pb	0.0075	2
^{208}Tl	0.831	8
^{207}Tl	3.1624	10

cay by "multiple preequilibrium" emission. Blann and Vonach [26] were the first to show the dramatic influence of multiple preequilibrium effects on $(p,2p)$ excitation functions. We found this mechanism to be important once the incident energy exceeds about 40 MeV, and it was included within an exciton model description [12]. As is shown by the calculations illustrated in Sec. V, the discrete γ-ray measurements presented here provide a very sensitive and interesting signature for the multiple preequilibrium process. The second modeling improvement was to calculate spin distributions for the residual states formed in preequilibrium reactions using angular momentum distributions based on the exciton model [27]. Previously, compound nucleus spin distributions were used for all reactions calculated in GNASH, including preequilibrium. And finally we have incorporated the excitation-energy dependence of the Ignatyuk level-density formula [23] into the particle-hole state densities used in the exciton model calculations.

Proton emission is only important in the precompound stage of the reaction; therefore the only proton-emitting reactions included in our calculations were the (n,p), (n,np), and $(n,2p)$ reactions, as emission of up to two preequilibrium particles is important at the higher energies. Proton emission from compound nucleus decay is negligible even for the most neutron-deficient Pb isotopes considered in our calculation, as the differences between proton and neutron separation energies are small compared to the height of the Coulomb barrier even for ^{200}Pb, the lightest isotope considered in our analysis.

Cross section calculations were performed with this *a priori* "best choice" parameter set and also with some modified parameter sets in order to illustrate the sensitivity of calculated cross sections to various model parameters as discussed in detail in the next section.

V. RESULTS AND DISCUSSION

Before our experiments, excitation functions for some of the γ transitions had only been measured between 5 and 9 MeV [13] and around 14 MeV. Our data for the ^{208}Pb 3_1^- $\rightarrow$gs transition are in good agreement with the results of Ref. [13] in the 5–9 MeV region (on average our cross sections are about 8% higher than those of Ref. [13], which is well within mutual uncertainty limits). There are big discrepancies between our data and most of the 14-MeV results which are probably caused by the use of very large samples with inadequate multiple scattering corrections in most of the 14-MeV experiments. This problem is discussed in detail in Ref. [5], describing the 14-MeV experiment performed by some of the authors for the absolute cross section normalization.

The main results of this work, the measured and calculated excitation functions for the prompt transitions between the lowest excited levels of ^{208,207,206,204,202,200}Pb and the ground states of these nuclei produced in ^{207,208}Pb($n,xn\gamma$) reactions, are shown in Figs. 4–12. Numerical values of the measured cross sections will be published in a separate laboratory report. These cross sections are from the population of specific low-lying levels by prompt transitions from higher-energy levels and by direct feeding in the particle emission process. If a level is fed from a higher-lying isomeric state, this part of the cross section is not included in our results. All of the Pb isotopes, except ^{208}Pb, have such isomers (see Sec. III, Table II). Correspondingly, the calculated cross sections are the differences between the calculated total population cross sections of the levels and the cross sections for the formation of the respective high-spin isomers decaying to the considered levels. In the case of the 2_1^+ $\rightarrow$gs transition in ^{204}Pb, the corresponding 899.1-keV γ line was not resolved from the 897.8-keV γ line from the decay of the first $\frac{1}{2}^-$ level of ^{207}Pb. Thus in this case the sum of these two cross sections is compared to the sum of the calculated cross sections. Because the neutron introduces considerable angular momentum, the population of the isomers is quite large, about 50–75 % of the total production cross sections of the various even-even

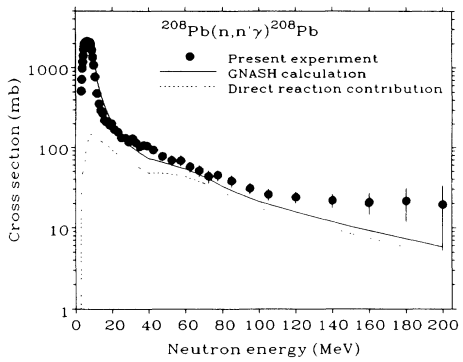

FIG. 4. Prompt ^{208}Pb($n,n'\gamma$)^{208}Pb cross section for the 3_1^- $\rightarrow$gs transition (E_γ = 2614.6 keV). Points with error bars: present experiment. Solid line: GNASH calculation with the standard parameter set. Dotted line: direct reaction contribution to the GNASH calculation.

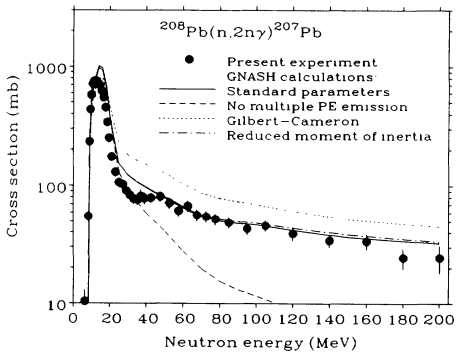

FIG. 5. Prompt ^{208}Pb($n,2n\gamma$)^{207}Pb cross section for the $(\frac{5}{2})_1^-$ $\rightarrow$gs transition (E_γ = 569.7 keV). Points with error bars: present experiment. Solid line: GNASH calculation with the standard parameter set. Dashed line: GNASH calculation without multiple preequilibrium (PE) emission. Dotted line: GNASH calculation using the Gilbert-Cameron level density. Dot-dashed line: GNASH calculation with the nuclear moment of inertia reduced to 60% of the rigid body value.

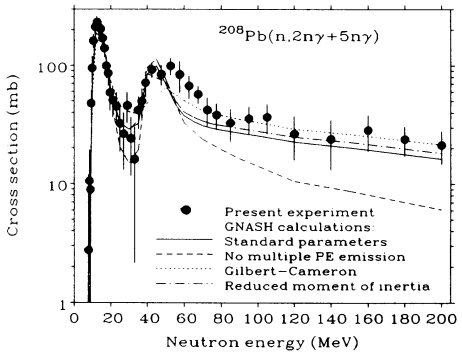

FIG. 6. Prompt ^{208}Pb$(n, 2n\gamma + 5n\gamma)$ cross section for the $(\frac{3}{2})^-_1$ →gs transition in ^{207}Pb (E_γ = 897.8 keV) and the 2^+_1 →gs transition (E_γ = 899.1 keV) in ^{204}Pb. Notation is the same as in Fig. 5.

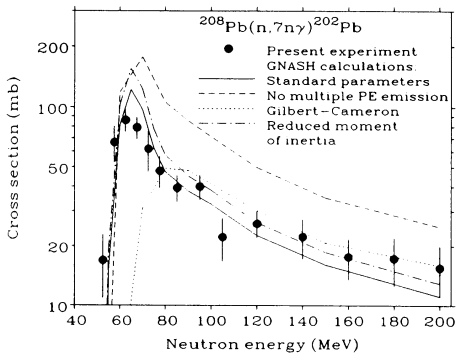

FIG. 8. Prompt ^{208}Pb$(n, 7n\gamma)^{202}$Pb cross section for the 2^+_1 →gs transition (E_γ = 960.7 keV) in ^{202}Pb. Notation is the same as in Fig. 5.

lead nuclei. Thus the prompt γ-production cross sections for the 2^+_1 levels of the even lead isotopes are essentially partial cross sections containing only 25–50 % of the total population of the respective residual nuclei, and are thus quite sensitive to details of the γ decay in the region of the discrete levels.

As seen in Figs. 4–12, there is reasonable agreement between our measurements and the calculations with our "standard parameter set," discussed in Sec. IV, over the whole energy range and for all of the different reactions. The agreement in the high-energy range, 100–200 MeV, seems to be even better than at lower energies; thus our results show that conventional preequilibrium Hauser-Feshbach calculations can be used successfully from low energies to at least 200 MeV, if multiple preequilibrium emission is properly taken into account and a realistic level density model is chosen. There are, however, some discrepancies, ranging from about 20% to a factor of 2, which need to be discussed in some detail.

(a) The $(n, n'\gamma)$ cross section for the 2615-keV 3^- →gs transition in ^{208}Pb [which represents almost the total (n, n') cross section] is considerably higher than calculated above about 100 MeV (see Fig. 4). At these energies, about 80% of the cross section is due to direct excitation of collective levels; thus this discrepancy must be related to the coupled-channels part of our calculations rather than the statistical model part. As the energy dependence of the coupled-channels cross section is well founded theoretically, the larger experimental cross section at higher energies is difficult to understand. It should be kept in mind, however, that our results for the cross section for the 2615-keV transition are rather uncertain at high energies because of the very large correction for finite sample effects (see Sec. III). Thus a considerable part of the discrepancy might be experimental; further measurements using a thinner ^{208}Pb target are needed to clarify the situation.

(b) There is some indication that for high-threshold reactions, e.g., $(n, 5n)$ to $(n, 9n)$ (see Figs. 8, 11, and 12), the cross section maximum above threshold, which is predominantly due to compound nucleus decay, is less pronounced than predicted theoretically. This indicates that there might be a somewhat broader distribution of excitation energies at the end of the precompound stage of the reaction than assumed in the calculations.

(c) There is some discrepancy between the results obtained from ^{208}Pb and ^{207}Pb concerning the cross sections for the same final 2^+_1 →gs transition in both ^{202}Pb and ^{200}Pb (see Figs. 8, 9, 11, and 12). In this case,

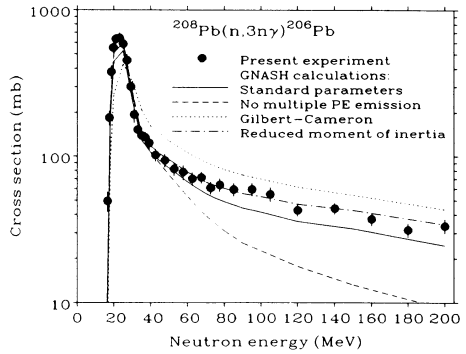

FIG. 7. Prompt ^{208}Pb$(n, 3n\gamma)^{206}$Pb cross section for the 2^+_1 →gs transition (E_γ = 803.1 keV) in ^{206}Pb. Notation is the same as in Fig. 5.

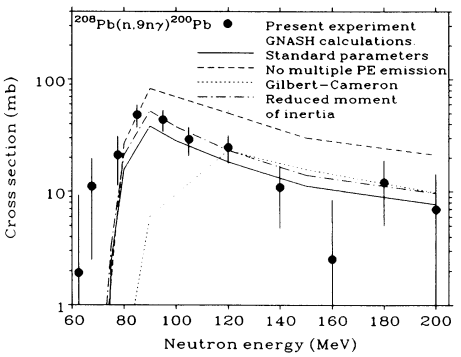

FIG. 9. Prompt ^{208}Pb$(n, 9n\gamma)^{200}$Pb cross section for the 2^+_1 →gs transition (E_γ = 1026.5 keV) in ^{200}Pb. Notation is the same as in Fig. 5.

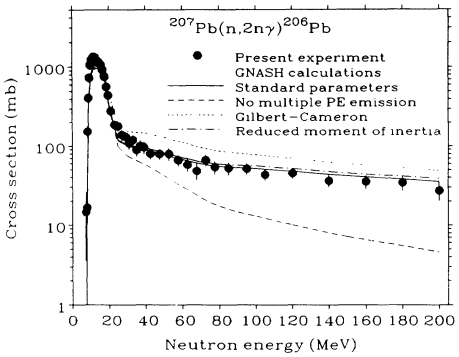

FIG. 10. Prompt ^{207}Pb($n,2n\gamma$)^{206}Pb cross section for the $2_1^+ \rightarrow$gs transition (E_γ = 803.1 keV) in ^{206}Pb. Notation is the same as in Fig. 5.

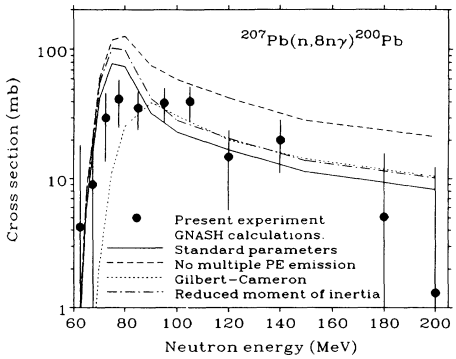

FIG. 12. Prompt ^{207}Pb($n,8n\gamma$)^{200}Pb cross section for the $2_1^+ \rightarrow$gs transition (E_γ = 1026.5 keV) in ^{200}Pb. Notation is the same as in Fig. 5.

one would expect that the calculated cross section ratios should be quite accurate because all uncertainties due to peculiarities in the decay scheme of the final nucleus should cancel. Nevertheless, in both cases the ^{207}Pb cross sections in the region of the maxima of the excitation functions are considerably smaller than calculated, whereas this effect is less pronounced in ^{208}Pb. Additional measurements on ^{206}Pb could contribute to a better understanding of this effect.

(d) Other smaller deviations between the experimental results and the calculations are in the usual range of discrepancies (within $\approx$ 20%) generally found for such calculations even at low energies.

In addition to the experimental results and the calculations with our "best choice" parameters, Figs. 5–12 also present a number of calculations which show the influence of different parameters on the calculated cross sections. These comparisons give some insight into the sensitivity of the calculated cross sections to the various parameters. In particular, results are shown for the following parameter variations:

(1) no multiple precompound emission,

(2) Gilbert-Cameron level density instead of the Ignatyuk model, and

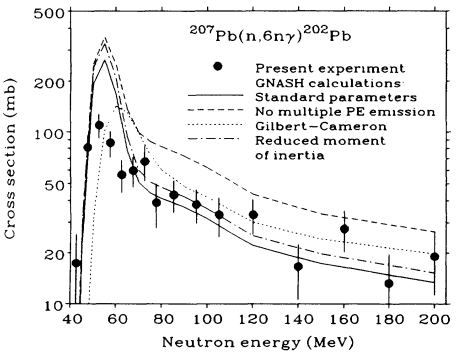

FIG. 11. Prompt ^{207}Pb($n,6n\gamma$)^{202}Pb cross section for the $2_1^+ \rightarrow$gs transition (E_γ = 960.7 keV) in ^{202}Pb. Notation is the same as in Fig. 5.

(3) nuclear moment of inertia reduced to 60% of the rigid body value.

The influence of multiple precompound particle emission manifests itself clearly in Figs. 5–12. Above neutron energies of about 40 MeV multiple precompound emission dramatically increases the $(n,2n)$ and $(n,3n)$ cross sections. As more high-energy neutrons are emitted, a larger fraction of the available incident energy is in two or three neutron emission steps, and correspondingly the cross sections for multiparticle emission decrease. The experimental data clearly support the precompound multiparticle emission model used in the GNASH code and indicate that it has to be used above $\approx$ 40 MeV incident energy.

The choice of the level density model influences the excitation functions in a more specific way. Its main effect is to shift the maxima of the excitation functions to higher energies (see Figs. 6–9, 11, and 12). The shift is negligible for the $(n,2n)$ reaction where the maximum cross section occurs around 15 MeV and rises to almost 30 MeV around the maximum of the $(n,9n)$ excitation function at 100 MeV. This effect can be understood as follows.

In the conventional level density formulas, the level density parameter a is determined at the neutron binding energy where it is strongly influenced by shell effects, and a is kept constant at higher excitation energies. In the Ignatyuk model, the more realistic assumption is made that low-energy shell effects disappear at excitation energies of $\approx$ 50 MeV. This gradual diminishing of the shell effects is described by an energy-dependent level density parameter which reaches an asymptotic value proportional to A at about 50 MeV excitation energy. For ^{208}Pb the a value at low excitation energy is only $\approx$ 10, whereas the asymptotic a value is about 20. This has the consequence that the nuclear temperature

$$T = \frac{1}{d(\ln\rho)/dU} \propto \left(\frac{U}{a}\right)^{1/2} \quad (1)$$

increases much faster with excitation energy U in the conventional models than in the Ignatyuk model (see

Fig. 13). [In Eq. (1) the proportionality is exact for the Gilbert-Cameron formula, but it is only approximate for the Ignatyuk formula.] At ≈ 100 MeV the difference in T between the two models is about 1.6 MeV. This temperature value determines the average energy of the emitted neutrons in the compound nucleus, $\bar{E}_{\rm kin} = 2T$. Considerably more energy per emitted neutron is predicted by the conventional model [24] than by the Ignatyuk model. This has the consequence that in the Gilbert-Cameron model considerably more energy is needed to produce a (n, xn) reaction with a specific x than in the Ignatyuk model. The result is that the effective threshold of a given (n, xn) reaction is shifted to higher energies in the Gilbert-Cameron model than in the Ignatyuk model. This behavior is demonstrated by the "Gilbert-Cameron" curves in Figs. 5–12. Because this shift is nearly proportional to the number of emitted neutrons times the temperature difference predicted by the two models (see Fig. 13), it increases almost quadratically with neutron energy (compare Figs. 6–9). Figures 8 and 9 show that our data clearly support the Ignatyuk model at energies above approximately 50 MeV, where low-energy shell effects in the level density disappear. In the transition region from 20 to 50 MeV the situation is not as clear. We have only one excitation function (see Fig. 6) with a cross section maximum in this energy range, and it has the complication that it was not separated from the excitation function for another γ transition of almost equal energy. Further studies γ transitions with excitation functions peaking in the 20–50 MeV range are needed to check in detail the behavior of the level density in the transition region between the low-energy and the asymptotic a-parameter values. This point will be specifically addressed in the continuation of this work.

The effect of changing the nuclear moment of inertia, which determines the value of the spin-cutoff parameter σ, was investigated. In addition to our standard calculation using the rigid body moment of inertia value, calculations were performed with a nuclear moment of inertia reduced to 60% of the standard value, with spin-cutoff factors reduced to about 80% of standard values. The consequence of this change is a higher probability for γ decay to levels of lower spins because relatively more such levels are present in the spin distribution. Thus, eventually the population of the high-spin isomers is decreased by a reduction of σ. Accordingly, the cross sections for γ decay via low-spin states, which is the experimentally observed quantity in Figs. 5–12, should increase. This effect can be seen in the figures, but quantitatively the effect is rather small. Our standard calculation seems to give somewhat better overall agreement, and thus no reduction of the nuclear moment of inertia is indicated by our data, but we cannot exclude the possibility of a reduced moment of inertia.

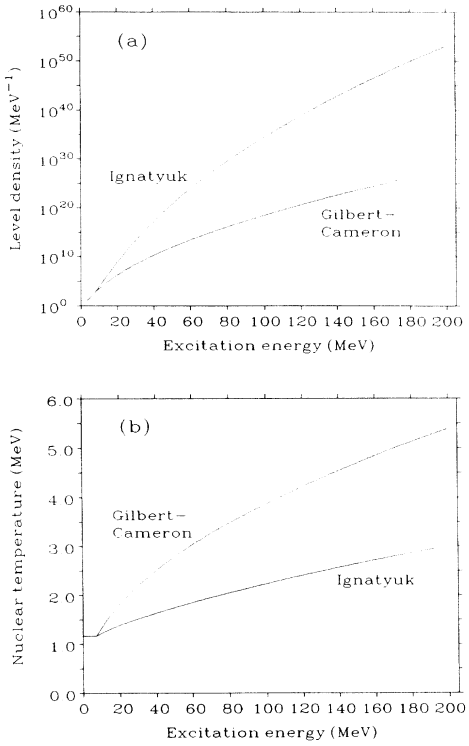

FIG. 13. Comparison of level densities according to Ignatyuk and Gilbert-Cameron models for ^{208}Pb: (a) level densities; (b) nuclear temperatures.

In summary, we have demonstrated the effectiveness of white source $(n, xn\gamma)$ measurements, in which prompt γ rays are detected, for supplying data that provide useful tests of nuclear models over a wide energy range. The calculations that we performed demonstrate the effectiveness of preequilibrium models at higher energies, and the importance of multiple preequilibrium particle emission and of the correct choice of the level density formulation to accurately describe the data.

ACKNOWLEDGMENTS

This work was supported by the Austrian Fonds zur Förderung der wissenschaftlichen Forschung (Project No. P7908-TEC), and the U.S. Department of Energy under Contracts No. W-7405-ENG-36 and No. W-7405-ENG-48.

[1] P. W. Lisowski, C. D. Bowman, G. J. Russell, and S. A. Wender, Nucl. Sci. Eng. **106**, 208 (1990).

[2] G. L. Morgan, T. A. Love, and F. G. Perey, Nucl. Instrum. Methods **128**, 125 (1975).

[3] J. K. Dickens, J. H. Todd, and D. C. Larson, "Cross Sections for Production of 70 Discrete-Energy Gamma Rays created by Neutron Interaction with ^{56}Fe for E_n to 40 MeV," Oak Ridge National Laboratory Report No.

ORNL/TM 11671, 1990; also J. K. Dickens, C. Y. Fu, D. M. Hetrick, D. C. Larson, and J. H. Todd, in *Proceedings of the International Conference on Nuclear Data for Science and Technology*, 1991, edited by S. M. Qaim (Springer-Verlag, Berlin, 1992), p. 307.

[4] R. O. Nelson, C. M. Laymon, and S. A. Wender, Nucl. Instrum. Methods Phys. Res. Sect. B **56**, 451 (1991).

[5] S. Hlaváč, P. Obložinský, L. Dostál, I. Turzo, H. Vonach, A. Pavlik, and S. Simakov, Nucl. Sci. Eng. (submitted).

[6] S. Hlaváč, P. Obložinský, and S. Simakov (private communication).

[7] S. A. Wender, S. Balestrini, A. Brown, R. C. Haight, C. M. Laymon, T. M. Lee, P. Lisowski, W. McCorkle, R. O. Nelson, and W. Parker, Nucl. Instrum. Methods Phys. Res. Sec. A **336**, 226 (1993).

[8] N. R. Yoder, "XSYS, IUCF Data Acquisition Software," Indiana University Cyclotron Facility internal report, 1991.

[9] P. W. Lisowski, A. Gavron, W. E. Parker, J. L. Ullmann, S. J. Balestrini, A. D. Carlson, O. A. Wasson, and N. W. Hill, "Fission Cross Sections in the Intermediate Energy Region," in Proceedings of the Specialists' Meeting on Neutron Cross Section Standards for the Energy Region above 20 MeV, Uppsala, Sweden, 1991, Nuclear Energy Agency Nuclear Data Committee Report No. NEANDC-305 'U', Paris, 1991, p. 177.

[10] C. M. Davisson, in *Alpha-, Beta- and Gamma-ray Spectroscopy*, edited by K. Siegbahn (North-Holland, Amsterdam, 1965), Vol. I, p. 827.

[11] ENSDF, The Evaluated Nuclear Structure Data File, Data received from National Nuclear Data Center, Brookhaven National Laboratory, 1993.

[12] P. G. Young, E. D. Arthur, and M. B. Chadwick, "Comprehensive Nuclear Model Calculations: Introduction to the Theory and Use of the GNASH Code," Los Alamos National Laboratory Report No. LA-12343-MS, 1992.

[13] J. K. Dickens, Nucl. Sci. Eng. **63**, 101 (1977).

[14] C. Kalbach, Z. Phys. A **283**, 401 (1977).

[15] C. Kalbach, Phys. Rev. C **32**, 1157 (1985).

[16] J. Kopecky and M. Uhl, Phys. Rev. C **42**, 1941 (1990).

[17] R. E. Shamu and P. G. Young, J. Phys. G **19**, L169 (1993).

[18] R. L. Schutt, R. E. Shamu, P. W. Lisowski, M. S. Moore, and G. L. Morgan, Phys. Lett. B **203**, 22 (1988).

[19] J. Raynal, "Optical Model and Coupled-Channels Calculations in Nuclear Physics," International Atomic Energy Agency Report No. IAEA SMR-9/8, Vienna, 1972, p. 281.

[20] R. E. Shamu and P. G. Young (private communication).

[21] F. D. Becchetti, Jr. and G. W. Greenlees, Phys. Rev. **182**, 1190 (1969).

[22] D. G. Madland, "Recent Results in the Development of a Global Medium-Energy Nucleon-Nucleus Optical-Model Potential," in Proceedings of the Specialists' Meeting on Preequilibrium Nuclear Reactions, Semmering, Austria, 1988, edited by B. Strohmaier, Nuclear Energy Agency Nuclear Data Committee Report No. NEANDC-245'U', Paris, 1988, p. 103.

[23] A. V. Ignatyuk, G. N. Smirenkin, and A. S. Tishin, Yad. Fiz. **21**, 485 (1975) [Sov. J. Nucl. Phys. **21**, 255 (1975)].

[24] A. Gilbert and A. G. W. Cameron, Can. J. Phys. **43**, 1446 (1965).

[25] P. G. Young, E. D. Arthur, M. Bozoian, T. R. England, G. M. Hale, R. J. LaBauve, R. C. Little, R. E. MacFarlane, D. G. Madland, R. T. Perry, and W. B. Wilson, Trans. Am. Nucl. Soc. **60**, 271 (1989); Los Alamos National Laboratory Report No. LA-11753-MS, 1990.

[26] M. Blann and H. K. Vonach, Phys. Rev. C **28**, 1475 (1983).

[27] M. B. Chadwick, P. G. Young, P. Obložinský, and A. Marcinkowski, Phys. Rev. C **49**, R2885 (1994).